Valley quantum Hall effect meets strain: Subgap formation and large increment of the Hall conductivity

A. Sinner [1,*] G. Engel [1] A. Ernst [2,3] and V. A. Stephanovich [1]
[1]*Institute of Physics, University of Opole, 45-052 Opole, Poland*
[2]*Max Planck Institute of Microstructure Physics, Weinberg 2, D-06120 Halle, Germany*
[3]*Institute for Theoretical Physics, Johannes Kepler University, Altenberger Straße 69, 4040 Linz, Austria*

(Received 20 July 2023; revised 23 October 2023; accepted 7 December 2023; published 22 December 2023)

We consider the effect of the uniaxial strain applied to a graphene monolayer with a realized quantum valley Hall state, for which we use a version of the Haldane model. In its specific point, the latter model has two spectral valleys: the gapless one and the gapped one. Using analytical and numerical arguments, we show that this state is unstable against mechanical deformations of the lattice, which influences the energy spectrum, the density of states, and the conductivity tensor. In particular, the Hall conductivity in the near-DC regime may surpass largely the known plateau value along with the simultaneous sign change. Above effects pave the way to the applied graphene strain engineering or *straintronics*. Namely, they can be used in quantum logical gates utilizing a controllable strain manipulation for reversing or on- and off-switching of the Hall current.

DOI: 10.1103/PhysRevB.108.235431

I. INTRODUCTION

Graphene is the thinnest material in the world, with only one layer of atoms arranged in a hexagonal (honeycomb) pattern. Because of that, it has many advantages for transparent and flexible electronics. Namely, it has high transparency [1–4], strong resistance to stress and bending [2,3] (it sustains reversible elastic deformations in excess of 20% [3,5]), and fast electron movement [5]. Graphene is considered as one of the most suitable materials for flexible devices like transpired conductive electrodes, bendable screens, e-paper, or clear solar cells [2,3]. However, to make this possible, we need to know how the electric and optical properties of graphene change when we apply voltage or pressure to it. Another interesting application of this technology is to make optical elements that can work with different wavelengths of light and that can be very small and easy to integrate with other devices. This is also a very important goal in the field of nanotechnology.

One of the simplest models which captures well the exceptional topological properties of graphene is the Haldane model [6]. The model was proposed by Haldane in his seminal 1988 work [6], based on the honeycomb lattice with nearest-neighbor and next-nearest-neighbor hopping. The model utilizes two key ingredients: a difference in the on-site energy of the two sublattices of graphene, which opens a gap in the band structure, and a staggered magnetic field that breaks the time-reversal symmetry of the system. The model shows that the system has nontrivial topological properties, such as a nonzero Chern number and chiral edge states, that depend on the sign and magnitude of the parameters. Due to the simplicity and physical elegance of the Haldane model [7], it is well-suited for our purposes of theoretical studies of the strain effects on graphene monolayers. The distinct feature of the Haldane model is that it does not require any external magnetic field to break the time-reversal symmetry. Instead, the broken time-reversal symmetry is mimicked by the absence of mirror symmetry between specific spectral structures within the Brillouin zone, the so-called valleys. Hence, the version of the quantum Hall effect described by the Haldane model is sometimes (and in this paper too) referred to as the *valley quantum Hall effect* [8]. The success of the model initiated subsequent intensive activities and led to the discovery of an entire class of related models based on different microscopic Hamiltonians, which share the same basic properties [9–11], and eventually became the object of experimental manipulations and engineering design [12].

The honeycomb lattice symmetries are the key component of the Haldane model. The excellent and robust transport properties of graphene are mainly due to the honeycomb symmetry of the underlying lattice which is responsible for salient spectral features. These and the transport properties can be manipulated and engineered by mechanical deformations of the honeycomb lattice, which has long been studied experimentally and theoretically [13,14]. The applied strain breaks the spatial isotropy of the honeycomb lattice. It displaces the spectral cones from their initial positions but does not alter the shape of the Brillouin zone [15–21]. The system reacts with modified spectral and transport properties. It is of considerable interest and intellectual challenge to investigate the properties of the Haldane-like models on mechanically deformed honeycomb lattices. The main questions which arise hereby are as follows: what are the effects of the modified topography of the honeycomb lattice on the spectra and the density of states (DOS); how does it affect the electronic transport in the system and in the longitudinal direction in particular; and to

*andreas.sinner@uni.opole.pl

what extent is the valley Hall state immune against the strain? These questions are also relevant for more complex systems composed of graphene monolayers. For instance, they are important for currently actively studied twisted graphene multilayers [22,23], where the strain leads to entirely unexpected effects [24,25].

This paper is devoted to the clarification of the above and other aspects in graphene and other valley quantum Hall systems. The main and quite unexpected result here is that the valley Hall state (corresponding to the situation with one solid and one fully gapped Dirac cone) turns out to be unstable towards the slightest violations of the spatial isotropy. As a consequence of that, the initially solid cone gets gapped and the system turns into an insulator with a large gaps mismatch. The comparison of the predictions made in our work with the results of realistic *ab initio* calculations [26] suggests that our model delivers pretty well a description of the strain effects in graphene and its results could be easily checked by currently available experimental methods and techniques.

The physical picture that unfolds in strained graphene is mainly the consequence of the above gaps mismatch. In what follows, we carry out a thorough investigation of different facets of strain influence like the gap evolution, the DOS, and different kinds of conductivity in the proposed model. The obtained physical picture enables us to envisage its possible applications in the spirit of the *straintronics* concept [26–29], e.g., the strain-engineered quantum Hall logical gates.

II. SPECTRAL AND TRANSPORT PROPERTIES OF ELECTRONS IN ANISOTROPIC HONEYCOMB LATTICE

In momentum space, the first quantized tight-binding Hamiltonian of electrons on a generic honeycomb lattice reads

$$\mathcal{H}_0 = -\sum_{j=1}^{3} \begin{pmatrix} 0 & t_j e^{ia_j\cdot k} \\ t_j e^{-ia_j\cdot k} & 0 \end{pmatrix}. \tag{1}$$

Here a_i are the nearest-neighbor positions on the honeycomb lattice:

$$a_1 = a(0,-1), \quad a_{2,3} = \frac{a}{2}(\pm\sqrt{3}, 1), \tag{2}$$

with a being the interatomic separation, which we be put to unity below. The Hamiltonian (1) has the 2×2 matrix structure in the sublattice space of the non-Bravais honeycomb lattice. Its energy spectrum consists of the following two bands:

$$\epsilon_\pm = \pm\epsilon, \quad \epsilon = \sqrt{h_1^2 + h_2^2}, \tag{3}$$

where

$$h_1 = -\sum_{i=1}^{3} t_i \cos(a_i\cdot k), \quad h_2 = -\sum_{i=1}^{3} t_i \sin(a_i\cdot k). \tag{4}$$

For an isotropic lattice, where all t_j are equal, both above spectral branches touch each other at six corners of the Brillouin zone,

$$b_1^\pm = \frac{4\pi}{3\sqrt{3}a}(\pm 1, 0), \tag{5}$$

$$b_2^\pm = \frac{2\pi}{3\sqrt{3}a}(-1, \pm\sqrt{3}), \tag{6}$$

$$b_3^\pm = \frac{2\pi}{3\sqrt{3}a}(1, \pm\sqrt{3}), \tag{7}$$

where they compose two full Dirac nodes. Near these points, the spectrum has a conical shape, where two cones are mirror copies of each other. Namely, they are mapped to each other by complex conjugation of the Hamiltonian and are, therefore, chiral. Alternatively, the above spectral structures are referred to as the spectral valleys. The violation of the mirror symmetry between them leads to the appearance of currents in the ground state and the onset of a quantum Hall state.

This picture is modified if the spatial isotropy is lifted and the hopping amplitudes t_j become different. This can be realized, for instance, by the application of the in-plane uniaxial mechanical strain. Such strain, acting on both sublattices in opposite directions, modifies the electronic hopping amplitude between the nearest atoms on the lattice. In terms of the effective Dirac description of graphene, this effect creates an additional term resembling the conventional vector potential, which, however, does not break the time-reversal symmetry of the Hamiltonian [15–18]. As we vary the strain (i.e., the electronic hopping amplitude t_j) continuously, the Dirac nodes can be moved in the momentum space accordingly. The main effects of this heuristic picture are captured by the simplified description, in which the hopping amplitudes t_2 and t_3 are kept fixed at the value t_0 of the isotropic lattice, while t_1 changes smoothly between t_0 and $2t_0$. This is the case of the uniaxial strain applied in the y direction. Then the Dirac cones with different chirality start moving in the momentum space towards each other along the following trajectory:

$$k_x = \pm\frac{2}{\sqrt{3}}\arccos\left[\frac{t}{2t_0}\right], \quad k_y = \pm\frac{2\pi}{3}. \tag{8}$$

At the particular value $t = 2t_0$, the Dirac nodes merge and give rise to an anisotropic spectrum with parabolic dispersion along the motion direction and linear perpendicular to it. This regime is known as the Lifshitz point. For larger t, the participating bands become separated by a gap. At the Lifshitz point, the spectral anisotropy turns into the transport anisotropy. In particular, the low-energy asymptotics of the DOS changes from $\sim E$ below the Lifshitz point (Dirac cone) to $\sim\sqrt{E}$ at this point [15]. Similar behavior of $\sigma_\perp \sim \sqrt{\omega}$ is demonstrated by the perpendicular (i.e., measured perpendicular to the strain application direction) optical conductivity as a function of external frequency ω. On the contrary, the parallel component of the optical conductivity diverges as $\sigma_\parallel \sim 1/\sqrt{\omega}$ [30,31]. At low energies, both components of the conductivity tensor are related by the so-called geometric average constrain [32–34]

$$\sqrt{\sigma_\parallel(\omega)\sigma_\perp(\omega)} \approx \sigma_0, \tag{9}$$

where σ_0 represents the frequency-independent, i.e., universal, conductivity of the isotropic system [35]. In the DC limit, the geometric average is satisfied for all strains between t_0

and $2t_0$ [30], the averaged quantity being the universal DC conductivity of graphene [36].

III. THE REALIZATION OF THE VALLEY SYMMETRY-BREAKING TERM

To realize our objectives, we implement the symmetry breaking between both valleys employing a version of the Haldane model [6,7] formulated in Ref. [11]. Technically, the valley symmetry breaking is realized by adding the term $h_3\sigma_3$, where σ_3 is the diagonal Pauli matrix with elements ± 1 and

$$h_3 = M\delta_{rr'} + t'\chi_{rr'}, \tag{10}$$

to the Hamiltonian (1). This term describes an inhomogeneous gap at both valleys. It is given here in the coordinate representation with summation over lattice site coordinates r and r'. Here M is the main gap value, and t' is the hopping amplitude between the second-nearest neighbors. The matrix element in the second term of Eq. (10) reads

$$\chi_{rr'} = \sum_{i=1,2,3} \left(e^{i\phi}\delta_{r',r+c_i} + e^{-i\phi}\delta_{r',r-c_i}\right), \tag{11}$$

where ϕ denotes the tunable Peierls phase of the periodic staggered magnetic field and c_i denotes the positions of the second-nearest neighbors on the honeycomb lattice:

$$c_1 = \sqrt{3}a(1,0), \quad c_{2,3} = \frac{\sqrt{3}a}{2}(-1, \pm\sqrt{3}). \tag{12}$$

As none of the vectors c_i are parallel or antiparallel to the strain application direction, the corresponding hopping amplitudes do not modify. In momentum space we have from Eq. (10)

$$h_3 = M + 2t'\sum_{i=1}^{3}\cos(c_i\cdot k + \phi). \tag{13}$$

In general, the term $h_3\sigma_3$ in the Hamiltonian (1) opens a gap in the dispersion

$$E_\pm = \pm E, \; E = \sqrt{h_1^2 + h_2^2 + h_3^2}. \tag{14}$$

The gap at each of the two valleys can be varied independently. In particular, it can be adjusted such that the gap parameter vanishes completely in one valley while remaining in the other. Sometimes this regime is called *the critical Haldane model* [6]. It is realized with the Peierls phase $\phi = -\pi/4$ and the fine-tuned main gap $M = 3t'(1+\sqrt{3})/\sqrt{2}$. Once this regime is established, the symmetry between the right- and left-handed Dirac cones is broken, and the system arrives at the nontrivial topological state with a finite Chern number,

$$C_1 = \frac{\mathrm{sgn}(M)}{2}, \tag{15}$$

which corresponds to the real part of the Hall conductivity $\mathrm{Re}\,\sigma_H = C_1\frac{e^2}{h}$. According to the prevailing lore, this quantity represents a universal topological invariant. In particular, it should not depend on the shape and width of the spectral band lying above the gap. According to this argumentation, if the second cone were gapped for some reason, it would also contribute to the Hall conductivity. The total Hall conductivity would then appear as the sum of both contributions, i.e., twice the value Eq. (15) or zero depending on the sign of the gap at each cone but irrespective of its size. The combination of the Haldane model with the uniaxial strain can thus give us a reliable tool for checking this fundamental claim, which is sometimes referred to as the TKNN theorem [37].

Under strain, the position of both valleys varies as in the case of simple honeycomb lattice. This process is shown in Fig. 1. Moreover, the strain also modifies the valleys of the Haldane model. Along the extremal trajectory (8), the expansion of the spectrum (14) causes the following changes:

(i) We get the presence of a zero-momentum gap at the originally gapless cone. We have in this case

$$h_3 = \frac{M}{6\sqrt{3}}[1 + 3\sqrt{3} + \tau^2 - 2\sqrt{4-\tau^2} - \tau(2+\sqrt{4-\tau^2})],$$
$$\tau = \frac{t}{t_0}. \tag{16}$$

For $\tau = 1$ it is zero, recovering the isotropic case. Expanding Eq. (16) in $\delta\tau = (t-t_0)/t_0 = \tau - 1$, we get

$$h_3 \sim \frac{3+\sqrt{3}}{18}M\delta\tau^2. \tag{17}$$

To distinguish it from the main gap of the Haldane model, we refer to this strain-induced gap as the *subgap* below.

(ii) Similarly, for the zero-momentum gap at the originally gapped cone, we get

$$h_3 = \frac{M}{6\sqrt{3}}[1 + 3\sqrt{3} + \tau^2 + 2\sqrt{4-\tau^2} - \tau(2-\sqrt{4-\tau^2})]. \tag{18}$$

For small $\delta\tau$, the main gap acquires the following strain-induced correction:

$$h_3 \sim M - \frac{3-\sqrt{3}}{18}M\,\delta\tau^2. \tag{19}$$

Hence, both gaps have the same sign $\mathrm{sgn}(M)$, irrespectively of the sign of $\delta\tau$. Since they are associated with cones with opposite chiralities, the corresponding Hall conductivities have different signs. The numerically evaluated subgap values at the originally gapless cone and gap corrections to the originally gapped cone are shown in Fig. 2.

IV. DENSITY OF STATES

To get insights into the physics of the critical Haldane model under strain, it is instructive to first consider the DOS, which is an imaginary part of the single-particle Green's function

$$\rho(E) = -\mathrm{Im}\,\mathrm{Tr}\int_{\mathrm{BZ}}\frac{d^2k}{4\pi^3}\,(H - E + i0^+)^{-1}. \tag{20}$$

Here, the trace operator Tr acts in the sublattice space and the momentum integral is to be taken over the Brillouin zone (BZ) of the honeycomb lattice. The numerical evaluation of the

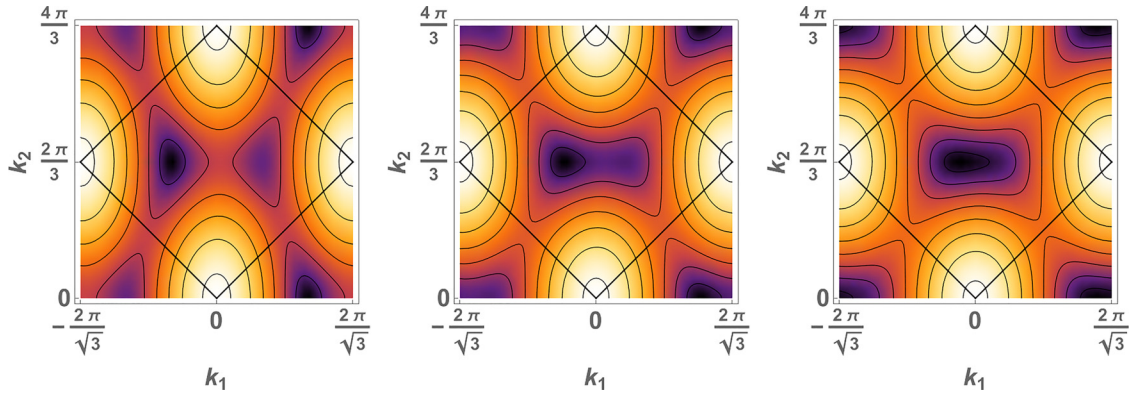

FIG. 1. The positions of the valleys in momentum space vs increasing parameter t/t_0 in the model with broken valley symmetry. The difference between valleys (large/small gap) and change of their locations are visually recognizable inside the black squares in the centers of the panels. Black squares (rhombi on real scale) in each panel show the plaquette used for the momenta summations, as explained in the text. Strain parameters from left to right: $t/t_0 = 1.0$, 1.5, and 2.0.

DOS shows that it combines several features inherent in both broken valley symmetry and lattice anisotropy. The effect of the former is most prominent in the low-energy domain. Since on isotropic lattice, the mass term defined in Eq. (13) gaps one of the cones, the low-energy contribution comes only from the second term. In particular, the slope of the linear part is only half of that of the full spectrum, and when the energy supersedes the gap in the other, the DOS changes abruptly, reaching the corresponding value of the full spectrum. The effects of the strain are twofold. First, similar to the isotropic lattices, it leads to the unpinning of the saddle points in the spectrum. In the DOS this effect generates the lower and higher van Hove singularities (Fig. 3). The appearance and origin of the multiple van Hove singularities have been previously noticed and discussed for the DOS in Refs. [16,19,34] and for the optical conductivity in Refs. [19,30,32]. Second, there is an effect that is specific to the Haldane model only. Namely, as we have discussed previously, the strain breaks the full cone in the spectrum and opens a gap. These gaps are visible in the DOS.

The numerical evaluation of the observables requires much caution. Namely, it is preferable to carry out the momentum integration not over the actual hexagonal Brillouin zone, which accounts for the cones at the corners only partly. This is the reason for the sizable spurious oscillations of the results. These issues become considerably less expressed if instead one integrates over the plaquette, which fully envelopes two opposing cones. This plaquette appears in Fig. 1 in the form of black rhombi. Such a rhombus has the same area as the conventional hexagonal Brillouin zone, is periodic in the reciprocal space, and can be used as a single element for covering the whole of it. Hence, the integration over this plaquette instead of the actual Brillouin zone does not influence the result. Still, the evaluated DOS (and later the conductivities) exhibit some noise, especially at higher energies (see Fig. 3). Importantly, this noise appears at higher energies and

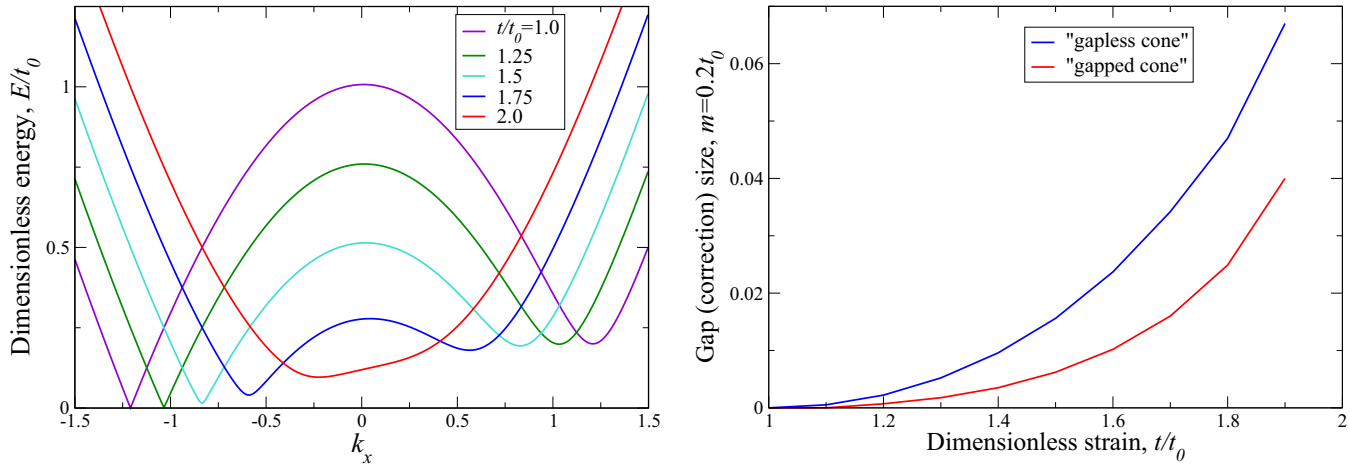

FIG. 2. Left panel: The spectrum of the model with broken valley symmetry under uniaxial strain. The left cone is gapless without strain but acquires a gap under strain. The right cone has the initial (i.e., for $t = 0$) gap $0.2t_0$. The strain values $1.0 < t/t_0 < 2.0$ are coded by colors and shown in the legend. As $t \to 2t_0$, the interminima separation becomes progressively smaller, and at the critical value $t = 2t_0$ they merge into a single one. Right panel: The size of the strain-induced subgap at the originally gapless left cone [blue line, Eq. (17)] and the main gap strain-induced correction [red line, Eq. (19)].

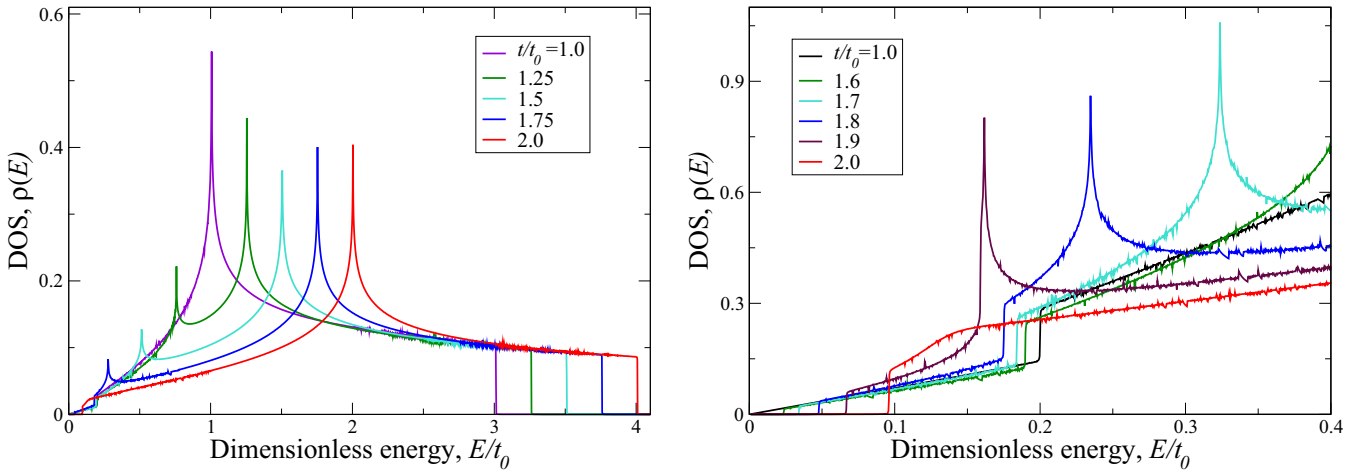

FIG. 3. The evolution of the DOS of the critical Haldane model with broken valley symmetry under strain. Left panel: General view of the DOS with the clearly visible splitting of the main van Hove singularity due to the unpinning of the saddle points in the spectrum at $t/t_0 > 1$. The strain values t/t_0 are similar to those in Fig. 2 (legend). Right panel: The low-energy part of the DOS at $E/t_0 < 0.4$. The strain values t/t_0 are shown in the legend. The second cone is gapped at arbitrarily small values of the strain, while the main gap acquires minimizing corrections by the strain, Eqs. (16) and (18). For $t/t_0 > 1.6$, the lower van Hove singularity enters the considered energy region. In both panels, the mass parameter is chosen to be $0.2t_0$.

is, therefore, largely indifferent to the value of the analytical continuation 0^+.

V. KUBO FORMULA FOR CONDUCTIVITY

The components of the conductivity tensor are calculated from the Kubo formula [38]

$$\sigma_{\mu\nu}(\omega) = \int_{\mathrm{BZ}} \frac{d^2k}{(2\pi)^2} \frac{f_\beta(E_k) - f_\beta(-E_k)}{2iE_k} \times \left(\frac{\mathrm{Tr}\{j_\mu \mathcal{P}_+ j_\nu \mathcal{P}_-\}}{\omega - 2E_k - i0^+} + \frac{\mathrm{Tr}\{j_\mu \mathcal{P}_- j_\nu \mathcal{P}_+\}}{\omega + 2E_k - i0^+} \right), \quad (21)$$

where $f_\beta(x)$ denotes the Fermi-Dirac distribution functions at inverse temperature $\beta^{-1} = k_B T$, with k_B being the Boltzmann constant. The projectors on the upper/lower band are defined as

$$\mathcal{P}_\pm = \frac{1}{2}\left[\mathbb{1} \pm \frac{\mathcal{H}}{E_k}\right]. \quad (22)$$

Here, the generic Hamiltonian is defined as

$$\mathcal{H} = h_1\sigma_1 + h_2\sigma_2 + h_3\sigma_3, \quad (23)$$

its spectrum $E_k = \sqrt{h_1^2 + h_2^2 + h_3^2}$, and the current operators are

$$j_\mu = \frac{\partial}{\partial k_\mu}\mathcal{H}, \quad (24)$$

where k_μ is wave vector in the $\mu = 1$ and 2 spatial directions. Using the notation $p_\nu^a = \frac{\partial h^a}{\partial k_\nu}$, the matrix element for generic h_i can be written as

$$\mathrm{Tr}\{j_\mu \mathcal{P}_\pm j_\nu \mathcal{P}_\mp\} = \frac{p_\mu^a p_\nu^b}{E_k^2}\left\{E_k^2\delta_{ab} - h_a h_b\right\} \mp i\epsilon_{abc}\frac{p_\mu^a p_\nu^b h^c}{E_k} \quad (25)$$

and applies to any matrix Hamiltonian of the form of Eq. (23), irrespective of its low-energy spectra.

Due to another numerical limitation, one has to ensure that the inverse quasiparticle lifetime 0^+ is actually kept finite but smaller than the frequency ω to avoid strong oscillations of the integrals. Unfortunately, because of this, the actual DC limit is not accessible as the frequency too needs to be kept finite.

VI. LONGITUDINAL CONDUCTIVITIES AND THE GEOMETRIC AVERAGE

We evaluate the longitudinal conductivity in the near-DC regime, i.e., for small constant external frequencies ω. One should be careful with that definition though, since it suggests the frequency-to-gap ratio to be small. While it is indeed possible to realize this for the main gap M of the model, there are always strain values for which the induced gap would be smaller than the frequency. Therefore, we expect the frequency-to-induced-gap ratio to vary gradually from very large values, passing through unity to the very small ones.

In both spatial directions, we observe a universal behavior of the real part of the corresponding longitudinal conductivity. This behavior is characterized by linear small-strain asymptotics with positive and negative slopes along and across the applied strain direction respectively. This asymptotics varies smoothly into a nonlinear increment and reaches a maximum before it abruptly breaks down at some scale.

The qualitative understanding of this behavior can be achieved with the help of the effective anisotropic Dirac Hamiltonian

$$H = v_1 k_1 \sigma_1 + v_2 k_2 \sigma_2 + m\sigma_3. \quad (26)$$

This Hamiltonian has the strain-dependent parameters $v_{1,2}$ and m. It captures well the physics of the originally gapless cone of the Haldane model for small strains. The current

operators become

$$j_{1,2} = v_{1,2}\sigma_{1,2}. \tag{27}$$

For the conductivity in the $\mu = 1$ direction, the matrix element in Eq. (25) becomes

$$\mathrm{Tr}\{j_\mu \mathcal{P}_\pm j_\nu \mathcal{P}_\mp\} = 4v_1^2 \frac{v_2^2 k_2 + m^2}{E_k^2}. \tag{28}$$

Then, for $\omega > 0$, we arrive at

$$\sigma_{11} = 2v_1^2 \int \frac{dk_1 dk_2}{(2\pi)^2} \frac{v_2^2 k_2^2 + m^2}{iE_k^3} \frac{1}{\omega - 2E_k - i0^+}. \tag{29}$$

Substituting $v_i k_i \to q_i$, we obtain the following for the real part:

$$\mathrm{Re}\ \sigma_{11} = \frac{v_1}{v_2} \int \frac{d^2q}{2\pi} \frac{q_2^2 + m^2}{E_q^3} \delta(2E_q - \omega). \tag{30}$$

The most convenient way to evaluate the integral (30) is to use the polar coordinates in the (q_1, q_2) plane. In this case, after performing the angular integration, we can replace $q_2^2 \to q^2/2$, integrate over q^2, and then integrate further over $E_q = \sqrt{q^2 + m^2}$. The final result is

$$\mathrm{Re}\ \sigma_{11} = \frac{v_1}{4v_2} \frac{\omega^2 + 4m^2}{\omega^2} \Theta(\omega - 2|m|). \tag{31}$$

To derive the expression (31), we exploited the properties of the Heaviside Θ function $\int_{|m|}^{\infty} dE = \int_{-\infty}^{\infty} \Theta(E - |m|)\, dE$. Analogously, we get the following for the perpendicular conductivity component:

$$\mathrm{Re}\ \sigma_{22} = \frac{v_2}{4v_1} \frac{\omega^2 + 4m^2}{\omega^2} \Theta(\omega - 2|m|), \tag{32}$$

which explains qualitatively the origin of the conductivity anisotropy in the strained system. The expressions (31) and (32) provide the qualitative understanding of the curves in Fig. 4. If there is no strain (i.e., $t/t_0 = 1$), when $m = 0$ and $v_i = v$ (v being the Fermi velocity of the isotropic lattice), the conductivities approach the same value

$$\mathrm{Re}\ \sigma_{\mu\mu} = \frac{1}{4}\frac{e^2}{\hbar} = \frac{1}{2}\sigma_0, \tag{33}$$

where we restore the conductivity units and the "universal" conductivity of the pristine graphene. At finite strain, i.e., for finite m, the system is conducting only for the frequencies larger than the double gap, i.e., for $\omega > 2|m|$. If the strain becomes so large that the frequency falls inside the gap, then the conductivity collapses to zero.

To reveal the main difference between the considered strained Haldane model and that of the "ordinary" graphene, it is useful to consider the geometric average

$$\sigma_{\mathrm{av}} = \sqrt{\sigma_{xx}\sigma_{yy}} \equiv \sqrt{\sigma_{11}\sigma_{22}}. \tag{34}$$

The comparison of the expression (34) with respect to Eqs. (31) and (32) shows the basic difference between the above two models. Namely, while the presented (strained Haldane) model has the frequency and strain-dependent σ_{av} (34), in the "ordinary" graphene this quantity has a strain-independent universal value (33) [30].

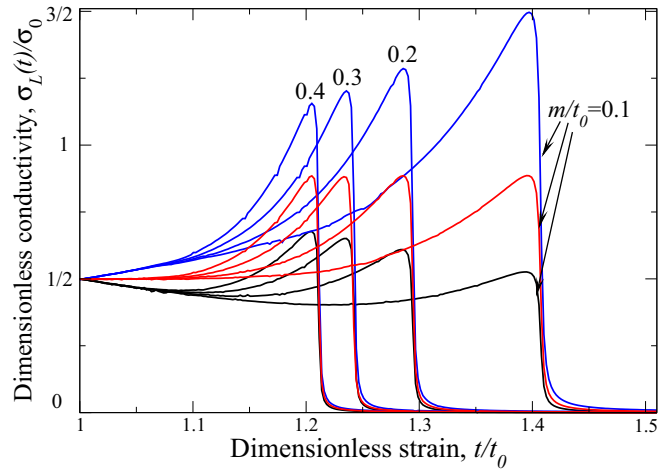

FIG. 4. The longitudinal conductivities parallel (yy components, blue curves) and perpendicular (xx components, black curves) to the strain direction. The conductivities are scaled in units of the universal conductivity of the isotropic system. The gap parameter is varied from $0.4t_0$ (maxima at smaller t/t_0) to $0.1t_0$ (maxima at larger t/t_0), see figures near the curves. The respective geometric averages are depicted in solid red. For smaller strains t/t_0, they collapse to a horizontal strain-independent line. The smaller the gap, the broader the strain-independent region. The frequency of the external field is chosen as $10^{-2}t_0$.

VII. HALL CONDUCTIVITY

The Hall conductivity of the critical Haldane model under strain is evaluated from the Kubo formula in a fashion similar to that of the longitudinal one. The near-DC results are reported in Fig. 5 and reveal several unexpected features. Namely, while the Hall conductivity starts at the universal value, inherent in unstrained graphene, at some quite small

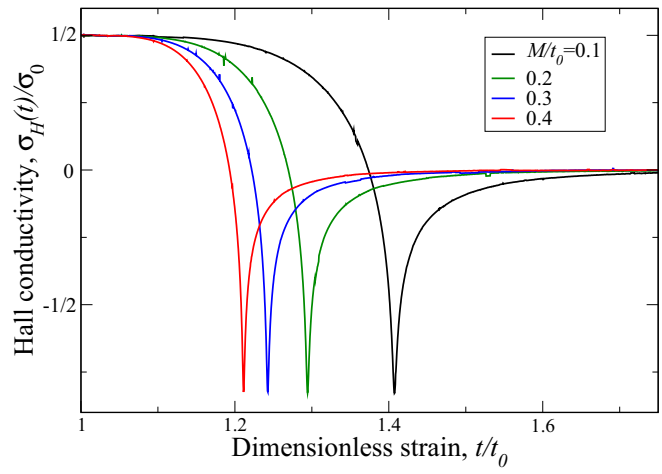

FIG. 5. The Hall conductivity in units of e^2/h calculated for different values of the main gap parameter M from Eq. (10) (legend). The visible behavior of the Hall conductivity is due to the interplay of the contributions from both cones. The TKNN regime is achieved for large strains, where the Hall conductivity approaches zero according to Eq. (35).

strains it decreases rapidly, switches the sign, develops a singularity, and finally approaches zero for larger strains.

The above behavior can also be understood with the help of the gapped Dirac Hamiltonian (26). To be more specific, it appears that this behavior is due to the combined effect of both cones:

$$\sigma_{\mathrm{H}}(t) = \sigma_{\mathrm{H}}^{M}(t) - \sigma_{\mathrm{H}}^{m}(t), \tag{35}$$

where $\sigma_{\mathrm{H}}^{M}(t)$ denotes the Hall conductivity contribution from the originally gapped cone and $\sigma_{\mathrm{H}}^{m}(t)$ denotes the Hall conductivity contribution from the originally gapless one. It reads specifically [11,39,40] as

$$\sigma_{\mathrm{H}}(t) \approx \frac{M(t)}{2\omega} \log\left|\frac{2M(t)+\omega}{2M(t)-\omega}\right| - \frac{m(t)}{2\omega} \log\left|\frac{2m(t)+\omega}{2m(t)-\omega}\right|. \tag{36}$$

We note that $M(t)$ depends weakly on the strain and can be assumed to be constant to the roughest approximation, similar to ω. The second term starts at zero, develops a singularity at $2m(t) = \omega$, and approaches the constant value for large t. The difference between both parts captures perfectly the shape of the conductivity in Fig. 5.

If the external frequency is initially chosen to be much smaller than the bare gap of the isotropic system, at the strain increase, the strain-induced subgap grows from being much smaller to much larger than the frequency. This interplay of different parameters crucially influences the Hall conductivity, which starts at the plateau related to the bare gap and then drops to zero at some threshold strain, where the Hall current is suppressed due to the synergy of the external field and strain. The threshold strain value can be estimated from Eq. (36): Assuming M to be constant and much larger than the frequency ω and introducing $x = m(t)/\omega$, we get the following at the zero point:

$$x_c \log\left|\frac{2x_c+1}{2x_c-1}\right| \approx 1. \tag{37}$$

The numerical solution is

$$m(t_c) \approx 0.41667\omega, \tag{38}$$

and then with Eq. (17) the critical strain

$$\delta\tau_c \approx 1.259\sqrt{\frac{\omega}{M}}. \tag{39}$$

With the strain increasing even further, the current reverses its direction; i.e., the Hall conductivity changes the sign. As the gap approaches the frequency (in energy units), the Hall conductivity increases dramatically due to the presence of highly populated states at the bottom of the spectral cone above the subgap [11]. With further strain increase, the subgap becomes comparable with the main gap, the valley symmetry gets restored, and the Hall conductivity tends to zero. According to Eq. (39), the TKNN regime [37] in the strained Haldane model sets up either in the *literal* DC limit, i.e., $\omega \to 0$, or in the *effective* DC regime, when $M \to \infty$. In both cases, the total Hall conductivity defined in Eq. (35) tends to zero, thus signaling the fulfillment of the TKNN theorem. Particularly in the second case this is because the strain-generated gap becomes much larger than the frequency $m(t) \gg \omega$ and the second term in Eq. (35) approaches the first. Therefore, the external frequency can be regarded as a measure of the deviation of the Hall conductivity from its topologically invariant value. However, since the TKNN theorem is formulated for the DC regime, there is no contradiction to our results. If any, the deviation from the TKNN theorem would be visible in the case $\omega/M \to 0$, but we do not observe any sizable effect here. Admittedly though, we have worked with the gaps *a priori* much smaller than the band width.

By varying the strain around the threshold value given in Eq. (39), one acquires a capability of controllable reversing of the Hall conductivity, which is tantamount to the same for the direction of the Hall current. With what has been said so far, we can indulge in envisioning a fascinating concept of a quantum Hall logical gate: a device based on strained graphene. This device would harness the discussed remarkable capabilities of a controllable reversing mechanism combined with an intricate on/off switching of the Hall current. These functionalities are achieved through precise and manipulable alterations in applied strain. Through this controllable manipulation, the device can effortlessly reverse the direction of its operations, defying the conventional logic.

VIII. DISCUSSION OF THE EXPERIMENTAL SITUATION AND CONTEXTS

The uniaxial strain applied to the pristine honeycomb lattice breaks its spatial isotropy by distinguishing a selected direction for electronic hopping. This emergent spatial anisotropy then passes through into the spectral and transport properties. This physics is well understood (see Ref. [41] and references therein).

On the other hand, here we consider the other mechanism of strain influence, which has not been considered to date. Namely, we consider the strain-induced violation of the symmetry between spectral valleys or Dirac cones. It opens a gap in the spectrum and thus turns the sample into a topologically nontrivial insulator. Recent experimental findings [42] show that, to generate the artificial magnetic field [see the expression (11) above] in a graphene sample, they need a strain around 3% of the initial lattice constant, which in our "hopping language" corresponds approximately to $t/t_0 = 1.4$ (see Supplemental Material of Refs. [42,43]). This artificial magnetic field is indeed related to the considered Haldane model [6] and is responsible for the effects, which we obtain theoretically (see Ref. [41] and references therein). This shows that the deformations in real graphene structures, at which the nontrivial patterns, related to the above artificial magnetic field appear, lie well within the parameters range used in our theoretical approach. As the aim of experimental research in Ref. [42] was not directly related to the quantities we have considered here, the precise experimental measurements of "ordinary" and Hall conductivities in strained graphene samples are badly needed.

Theoretically, the symmetry breaking between spectral valleys is realized by the inclusion of the Haldane-like term in the initial system Hamiltonian (1). At a specific point of the model, only one of the Dirac cones inside the Brillouin

zone is gapped while the other remains solid. At this point the system exhibits both the longitudinal and the transversal (Hall) conductivities, both taking exact quantized values dictated by the spectral topology of the model. The "marriage" of both models reveals a fascinating interplay of each model's features, clearly visible in observable quantities. The critical regime happens to be very fragile with respect to mechanical distortion. No matter how weak the strain is, the only solid cone of the critical Haldane model gets broken and acquires a spectral gap, even though it might seem negligible for small strains, because of the quadratic dependence. On the other hand, at the gapped node, the strain tries to reduce the bare gap. As the strain increases, the system evolves towards a state with a gap at each cone comparable in size. As the presence of a single gap in the critical Haldane model manifests the broken time-reversal symmetry, the gap equalization process might be considered as the natural tendency of the system towards a more trivial state with higher symmetry. The appearance of the subordinated subgap and the modification of the main gap are clearly visible in the DOS. Since the DOS is a normalized quantity, the disappearance of the low-energetic states due to the subgap opening is compensated by the emergence of additional states below the main gap edge (Fig. 3).

The nontrivial topology of the electronic spectrum on a honeycomb lattice is reflected in a number of perfectly quantized observables, mainly the DC longitudinal (universal) and transversal (Hall plateau) conductivities. The universal conductivity is a fundamental invariant of the isotropic system, closely related to the topology of the spectrum. Even if the spatial isotropy of the system is violated, it can be reconstructed in the process called the geometric average. Formally, it is given by Eq. (9) and states that the product of optical (i.e., frequency dependent) conductivities measured along and across the strain application direction is a universal, frequency-independent quantity with the precise value of the universal conductivity. Moreover, the geometric average is also strain independent. The latter property turns out to be also valid for the strained critical Haldane model, as long as the induced subgap does not supersede the external frequency (Fig. 4). The conductivity breaks down when the subgap becomes larger than the external frequency.

The Hall conductivity reveals a spectacular behavior. If the external frequency is initially chosen to be much smaller than the bare gap of the isotropic system, at the strain increase, the strain-induced subgap grows from being much smaller to much larger than the frequency. This interplay of different parameters crucially influences the Hall conductivity, which starts at the plateau related to the bare gap, then drops to zero at some threshold strain, where the Hall current is suppressed, and changes the sign for larger strain values.

According to the *ab initio* simulations of graphene performed by Choi *et al.* in Ref. [26] (and verified and improved by several others since), the shift of Dirac points should be indeed observed for the strains as small as 8% increase of the interatomic distance. Also, the merging of cones, i.e., the Lifshitz transition, has been predicted there at the strain of 26.5%, which in our units corresponds approximately to 2.2, which is quite close to our threshold value $t/t_0 = 2$ (see also above). Recent reviews [27,41] list similar values for several graphene-like materials, including silicene, phosphorene, etc. Therefore, our theoretical model should be well within reach of currently available experimental techniques.

The theoretically predicted physical picture enables us to devise a *straintronic* quantum Hall gate, i.e., a Hall current switching microelement functioning with the help of the strain. By employing carefully calibrated adjustments to the strain, the gate gains the remarkable ability to seamlessly toggle the flow of the Hall current on and off. This extraordinary feat allows for unprecedented control over the device's functionality and opens up endless possibilities for data manipulation and processing. While this speculation stretches the bounds of current scientific understanding, it ignites the imagination and invites us to envision a future where such strained-graphene-based devices might exist, captivating the world with their unparalleled capabilities and paving the way for exciting advancements in the realm of quantum logic and technology.

ACKNOWLEDGMENTS

The Opole group acknowledges support by Grant No. JSF-22-10-0001 of the Julian Schwinger Foundation for Physics Research. A.S. acknowledges the long-term collaboration on related topics with Prof. K. Ziegler, University of Augsburg. Fruitful discussions with Prof. F. Guinea and Dr. P. Pantanleón, IMDEA Nanosciencia Madrid, are gratefully appreciated. A.E. acknowledges funding by the Fonds zur Förderung der Wissenschaftlichen Forschung (FWF) under Grant No. I 5384.

[1] A. K. Geim, Graphene: Status and prospects, Science **324**, 1530 (2009).

[2] S. Bae, H. Kim, Y. Lee, X. Xu, J.-S. Park, Y. Zheng, J. Balakrishnan, T. Lei, H. R. Kim, Y. I. Song, Y.-J. Kim, K. S. Kim, B. Özyilmaz, J.-H. Ahn, B. H. Hong, and S. Iijima, Roll-to-roll production of 30-inch graphene films for transparent electrodes, Nat. Nanotechnol. **5**, 574 (2010).

[3] K. I. Bolotin, K. J. Sikes, Z. Jiang, M. Klima, G. Fudenberg, J. Hone, P. Kim, and H. L. Stormer, Ultrahigh electron mobility in suspended graphene, Solid State Commun. **146**, 351 (2008).

[4] R. R. Nair, P. Blake, A. N. Grigorenko, K. S. Novoselov, T. J. Booth, T. Stauber, N. M. R. Peres, and A. K. Geim, Fine structure constant defines visual transparency of graphene, Science **320**, 1308 (2008).

[5] F. Liu, P. Ming, and J. Li, *Ab initio* calculation of ideal strength and phonon instability of graphene under tension, Phys. Rev. B **76**, 064120 (2007).

[6] F. D. M. Haldane, Model for a quantum Hall effect without Landau levels: Condensed-matter realization of the "parity anomaly," Phys. Rev. Lett. **61**, 2015 (1988).

[7] F. D. M. Haldane, Nobel lecture: Topological quantum matter, Rev. Mod. Phys. **89**, 040502 (2017).

[8] Y. Ren, Z. Qiao, and Q. Niu, Topological phases in two-dimensional materials: A review, Rep. Prog. Phys. **79**, 066501 (2016).

[9] B. A. Bernevig, T. L. Hughes, and S.-C. Zhang, Quantum spin Hall effect and topological phase transition in HgTe quantum wells, Science **314**, 1757 (2006).

[10] C. L. Kane and E. J. Mele, Quantum spin Hall effect in graphene, Phys. Rev. Lett. **95**, 226801 (2005).

[11] A. Hill, A. Sinner, and K. Ziegler, Valley symmetry breaking and gap tuning in graphene by spin doping, New J. Phys. **13**, 035023 (2011).

[12] G. Jotzu, M. Messer, R. Desbuquois, M. Lebrat, T. Uehlinger, D. Greif, and T. Esslinger, Experimental realization of the topological Haldane model with ultracold fermions, Nature (London) **515**, 237 (2014).

[13] Y. Jiang, J. Mao, J. Duan, X. Lai, K. Watanabe, T. Taniguchi, and E. Y. Andrei, Visualizing strain-induced pseudomagnetic fields in graphene through an hBN magnifying glass, Nano Lett. **17**, 2839 (2017).

[14] M. A. H. Vozmediano, M. I. Katsnelson, and F. Guinea, Gauge fields in graphene, Phys. Rep. **496**, 109 (2010).

[15] Y. Hasegawa, R. Konno, H. Nakano, and M. Kohmoto, Zero modes of tight-binding electrons on the honeycomb lattice, Phys. Rev. B **74**, 033413 (2006).

[16] B. Wunsch, F. Guinea, and F. Sols, Dirac-point engineering and topological phase transitions in honeycomb optical lattices, New J. Phys. **10**, 103027 (2008).

[17] V. M. Pereira, A. H. Castro Neto, and N. M. R. Peres, Tight-binding approach to uniaxial strain in graphene, Phys. Rev. B **80**, 045401 (2009).

[18] G. Montambaux, F. Piéchon, J.-N. Fuchs, and M. O. Goerbig, Merging of Dirac points in a two-dimensional crystal, Phys. Rev. B **80**, 153412 (2009).

[19] F. M. D. Pellegrino, G. G. N. Angilella, and R. Pucci, Strain effect on the optical conductivity of graphene, Phys. Rev. B **81**, 035411 (2010).

[20] M. Oliva-Leyva and G. G. Naumis, Understanding electron behavior in strained graphene as a reciprocal space distortion, Phys. Rev. B **88**, 085430 (2013).

[21] M. Oliva-Leyva and G. G. Naumis, Generalizing the Fermi velocity of strained graphene from uniform to nonuniform strain, Phys. Lett. A **379**, 2645 (2015).

[22] Y. Cao, V. Fatemi, S. Fang, K. Watanabe, T. Taniguchi, E. Kaxiras, and P. Jarillo-Herrero, Unconventional superconductivity in magic-angle graphene superlattices, Nature (London) **556**, 43 (2018).

[23] Y. Cao, V. Fatemi, A. Demir, S. Fang, S. L. Tomarken, J. Y. Luo, J. D. Sanchez-Yamagishi, K. Watanabe, T. Taniguchi, E. Kaxiras, R. C. Ashoori, and P. Jarillo-Herrero, Correlated insulator behaviour at half-filling in magic-angle graphene superlattices, Nature (London) **556**, 80 (2018).

[24] A. Sinner, P. A. Pantaleón, and F. Guinea, Strain-induced quasi-1D channels in twisted moiré lattices, Phys. Rev. Lett. **131**, 166402 (2023).

[25] F. Escudero, A. Sinner, Z. Zhan, P. A. Pantaleón, and F. Guinea, Designing moiré patterns by strain, arXiv:2309.08671.

[26] S.-M. Choi, S.-H. Jhi, and Y.-W. Son, Effects of strain on electronic properties of graphene, Phys. Rev. B **81**, 081407(R) (2010).

[27] G. G. Naumis, S. Barraza-Lopez, M. Oliva-Leyva, and H. Terrones, Electronic and optical properties of strained graphene and other strained 2D materials: A review, Rep. Prog. Phys. **80**, 096501 (2017).

[28] I. Y. Sahalianov, T. M. Radchenko, V. A. Tatarenko, G. Cuniberti, and Y. I. Prylutskyy, Straintronics in graphene: Extra large electronic band gap induced by tensile and shear strains, J. Appl. Phys. **126**, 054302 (2019).

[29] J. M. Kim, M. F. Haque, E. Y. Hsieh, S. M. Nahid, I. Zarin, K.-Y. Jeong, J.-P. So, H.-G. Park, and S. Nam, Strain engineering of low-dimensional materials for emerging quantum phenomena and functionalities, Adv. Mater. **35**, 2107362 (2023).

[30] K. Ziegler and A. Sinner, Lattice symmetries, spectral topology and opto-electronic properties of graphene-like materials, Europhys. Lett. **119**, 27001 (2017).

[31] P. Nualpijit, A. Sinner, and K. Ziegler, Tunable transmittance in anisotropic two-dimensional materials, Phys. Rev. B **97**, 235411 (2018).

[32] V. M. Pereira, R. M. Ribeiro, N. M. R. Peres, and A. H. C. Neto, Optical properties of strained graphene, Europhys. Lett. **92**, 67001 (2010).

[33] J. P. Carbotte, K. R. Bryenton, and E. J. Nicol, Optical properties of a semi-Dirac material, Phys. Rev. B **99**, 115406 (2019).

[34] J. P. Carbotte and E. J. Nicol, Signatures of merging Dirac points in optics and transport, Phys. Rev. B **100**, 035441 (2019).

[35] Z. Q. Li, E. A. Henriksen, Z. Jiang, Z. Hao, M. C. Martin, P. Kim, H. L. Stormer, and D. N. Basov, Dirac charge dynamics in graphene by infrared spectroscopy, Nat. Phys. **4**, 532 (2008).

[36] K. S. Novoselov, A. K. Geim, S. V. Morozov, D. Jiang, M. I. Katsnelson, I. V. Grigorieva, S. V. Dubonos, and A. A. Firsov, Two-dimensional gas of massless Dirac fermions in graphene, Nature (London) **438**, 197 (2005).

[37] D. J. Thouless, M. Kohmoto, M. P. Nightingale, and M. den Nijs, Quantized Hall conductance in a two-dimensional periodic potential, Phys. Rev. Lett. **49**, 405 (1982).

[38] R. Kubo, Statistical-mechanical theory of irreversible processes. I. General theory and simple applications to magnetic and conduction problems, J. Phys. Soc. Jpn. **12**, 570 (1957).

[39] R. Nandkishore and L. Levitov, Spontaneously ordered states in bilayer graphene, Phys. Scr. **T146**, 014011 (2012).

[40] A. Hill, A. Sinner, and K. Ziegler, Optical Hall conductivity of systems with gapped spectral nodes, Eur. Phys. J. B **86**, 53 (2013).

[41] B. Amorim, A. Cortijo, F. de Juan, A. G. Grushin, F. Guinea, A. Gutiérrez-Rubio, H. Ochoa, V. Parente, R. Roldán, P. San-Jose, J. Schiefele, M. Sturla, and M. A. H. Vozmediano, Novel effects of strains in graphene and other two dimensional materials, Phys. Rep. **617**, 1 (2016).

[42] Y.-W. Liu, Z. Zhan, Z. Wu, C. Yan, S. Yuan, and L. He, Realizing one-dimensional electronic states in graphene via coupled zeroth pseudo-Landau levels, Phys. Rev. Lett. **129**, 056803 (2022).

[43] H. Shi, Z. Zhan, Z. Qi, K. Huang, E. van Veen, J. A. Silva-Guillén, R. Zhang, P. Li, K. Xie, H. Ji, M. I. Katsnelson, S. Yuan, S. Qin, and Z. Zhang, Large-area, periodic, and tunable intrinsic pseudo-magnetic fields in low-angle twisted bilayer graphene, Nat. Commun. **11**, 371 (2020).